Optical Properties and Analysis of OJL Model's Electronic inter-band Transition Parameters of TiO_2 Films

Nicholas Musila [1], **Mathew Munji** [1], **Justus Simiyu** [2], **Eric Masika** [1], **Raphael Nyenge** [1]

[1] *Kenyatta University*
P. O. Box 43844-00100, Nairobi, Kenya

[2] *University of Nairobi*
P. O. Box 30197-00100, Nairobi, Kenya

DOI: 10.22178/pos.36-5

LCC Subject Category: TP155-156

Received 20.06.2018
Accepted 20.07.2018
Published online 31.07.2018

Corresponding Author:
Nicholas Musila
musila.nicholas@ku.ac.ke

Abstract. Titanium dioxide is a wide band gap semiconductor responsible for the bright white appearance in most substances. This material has many unique properties due to its extra-ordinary chemical stability. TiO_2 has a conduction band that closely matches the excited energy level of organic dyes hence it is used in fabrication of photo-anode electrode of dye sensitized solar cell. However, the optical properties and the density of states of TiO_2 thin films determine the performance of dye sensitized solar cell fabricated from TiO_2 photo-anode electrode. For this reason, the purpose of this study was to investigate the optical properties and the OJL electronic inter-band transition analysis of TiO_2 nanoparticle thin films. Under the OJL model, the expressions of density of states were specified for the optical transition from the valence band to the conduction band. The TiO_2 nanoparticles were prepared using sol-gel and hydrothermal methods and deposited on a conductive glass substrate by screen printing and spray pyrolysis techniques. SEM analysis revealed that TiO_2 nanoparticles were spongy and had unevenly sphere-shaped profile while TiO_2 nanotubes had a skein-like morphology with abundant number of nanotubes intertwined together. This study showed that TiO_2 thin films have both direct and indirect band-gaps. The OJL Gap energy (E_0) values were observed to be between 30273.2356 and 31072.0000 wavenumbers which translated to band-gap energies between 3.744 and 3.843 eV. From these findings showed that TiO_2 films prepared could be used in the fabrication of high performing dye-sensitized solar cell.

Keywords: TiO_2 nanotube thin films, density of states, OJL model parameters, OJL Gap energy, spray pyrolysis.

INTRODUCTION

TiO_2 is a semiconductor material that is cheap and easily available [1]. TiO_2 is widely used in pigments and paints. Since it is non-toxic, it is used in food production industries [2], cosmetics and hygienic products [3]. TiO_2 occurs in three main crystalline forms namely anatase, rutile and brookite [4]. For DSSCs fabrication, the anatase crystalline structure is the most suitable [5]. The usual TiO_2 nanoparticle dimension to be used as DSSC's photo-anode electrode film is 10–30 nm [6].

Several deposition techniques have been used to prepare TiO_2 films which include screen printing [7], sol-gel [8], sputtering [9], chemical vapor deposition [10] and electrophoretic [11]. Sol-gel technique is the utmost popular since it's easy in the preparation of the nanoxide films. In addition, TiO_2 powders prepared though sol-gel have high catalytic activity owing to their large surface area, fine structure and high porosity [12].

The optical properties and the density of states of TiO_2 thin films, among other factors, determine the performance of dye sensitized solar cell fabricated from TiO_2 photo-anode electrode. On this basis, the main aim of this study was to report on the optical properties, OJL model parameters and SEM analysis of TiO_2 thin films synthesized using sol-gel and hydrothermal methods. The fabricated thin films were optically characterized from which the OJL parameters were determined from transmittance data obtained. SEM analysis was done so as to confirm their morphology.

Optical transmission and reflectance

Photons of selected wavelengths and beam intensity I_o (photons/cm^2) are directed at the film.

Those with energies greater than band gap (E_g) are absorbed while those with energies less than E_g are transmitted. This is because photons with energy less than band gap do not excite electrons in the valence band to higher states, hence transmitted. The comparison between intensities of incident (I_o) and transmitted (I_t) photons is given by transmittance. Transmittance is given by Equation 1:

$$Transmittance\ (T) = \frac{I_t}{I_o} \quad (1)$$

When light is passed across a material, it's expected that it does not get scattered. However, internal reflections of the light take place on the medium surface. For this reason, sampling of gases, liquids and solids is performed by transmission spectroscopy where the ratio of the transmitted light against the incident light is considered. This ratio is dependent on several factors like light path-length (thickness of the sample), the sample's reflectivity, the sample's absorption coefficient, the orientation of the particles in the sample, sizes of the particles in the sample and the light's incidence angle.

Reflectance is the percentage measure of ratio of intensity of incident light to that of reflected light. In the spectrophotometer, incident light of known wavelength and intensity is shone onto the surface of thin film and the intensity of reflected light measured. The two intensities are compared by reference called reflectance (R) as given in Equation 2:

$$R = \frac{I_R}{I_o} \times 100 \quad (2)$$

where I_R and I_o are intensities of the reflected and incident beams respectively.

The OJL model

OJL inter band model has been used to describe inter band transition in crystalline materials. It provides the equations for the density of states for the optical transition from the valence band to conduction band. Parabolic bands are assumed with tail states exponentially decaying into the band gap. The original parameters of OJL density of states model are energy, E_v and E_c, and the 'damping constants' of the conduction and valence bands, γ_c and γ_v. In addition, the conduction band mass, m_c and the valence band mass, m_v are included (Equations 3, 4):

$$E_{M.C} = E_C + \frac{1}{2}\gamma_C \quad (3)$$

$$E_{M.V} = E_V - \frac{1}{2}\gamma_V \quad (4)$$

Its represent the mobility edges of conduction and the valence bands.

The band gap, E_o, is consequently specified by [14]:

$$E_C + \frac{1}{2}\gamma_C - \left[E_V - \frac{1}{2}\gamma_V\right] = E_O \quad (5)$$

The band gap energy (E_o) is calculated by scout programme which converts the wave numbers to energy (eV). The other OJL electronic inter-band transition parameters are the OJL decay, OJL Mass, the OJL Gamma valence band, and the OJL Ratio.

Experimental procedure

The TiO_2 organic solution for TiO_2 nanoparticle films was synthesized at room temperature using sol-gel method where 1 ml of 2-propanol (Aldrich anhydrous 99.9 %) was mixed with 3.7 ml titanium (IV) isopropoxide (Aldrich 99.9 %) in volume. 2-propanol solution was added dropwise for over 30 minutes into a mixture of 25 ml of water and 8 ml glacial acetic acid (Aldrich 99.9%) and stirred vigorously for 1 hour. The mixture was there-after heated to 80 °C, stirred magnetically for 8 hours and then allowed to cool. Commercial TiO_2 nanotube powder was purchased from Sigma Aldrich and dissolved in ethanol to form a paste.

TiO_2 thin films were coated on FTO glass by screen printing and spray pyrolysis methods and dried in an oven at 80 °C for 10 minutes. Some TiO_2 nanotubes films were treated with titanium tetrachloride. The films were sintered in a furnace at 450 °C for 30 minutes. After annealing TiO_2 films at 450 °C, they were mounted on a holder inserted in the scanning electron microscope (Carl Zeiss Sigma VP FE-SEM). The voltage

was set at 6 kV and the working distance was set at 5.1 mm for the nanoparticle films and 10 kV and 3 mm for the nanotube film.

Shimadzu 3700 DUV UV-VIS-NIR Spectrophotometer was used to determine the optical characteristics of thin films. Transmittance and reflectance data at 200 nm to 1200 nm wavelength was collected. Drude model was used in optical constants analysis where the adjusted parameters included plasma frequency, damping constant and charge carrier density. For inter-band transitions, the OJL model as decay, gap energy and gamma were the varied parameters. Harmonic Oscillator was used to obtain the plasma frequency [18]. Transmittance measurements were fixed to the simulated spectra where film thickness, absorption coefficients and energy band gaps of thin films were obtained. The film thicknesses obtained from the scout software were compared to the thicknesses determined by the KLA-Tencor *Alpha-Step* IQ Surface *Profilometer*.

RESULTS AND DISCUSSION

SEM analysis. The micrograph of TiO_2 compact layer is represented in Figure 1.

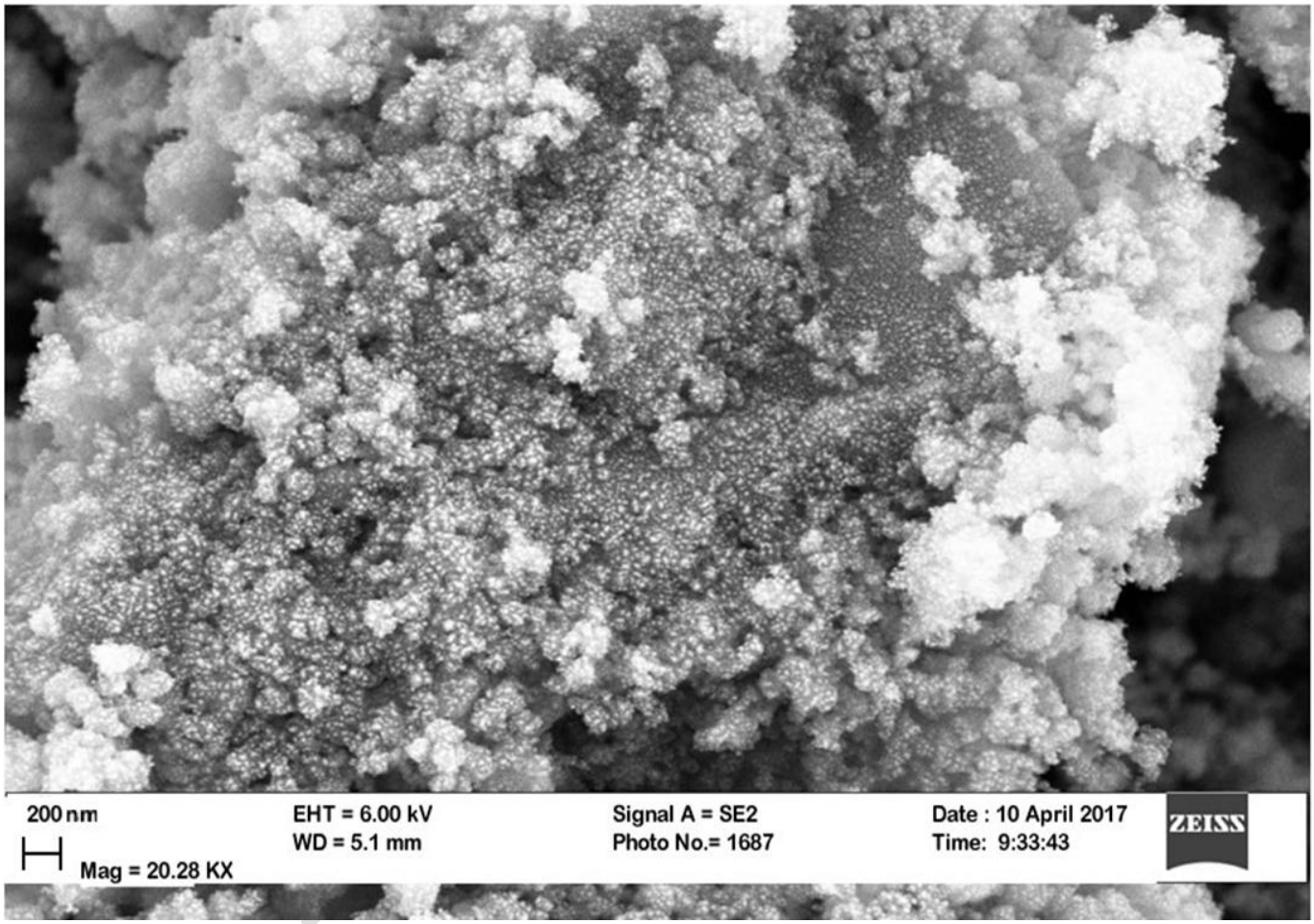

Figure 1 – SEM micrograph of titanium dioxide compact layer

It was noted that the film had a relatively uniform thickness owing to the deposition method used. The film was relatively smooth because of the slight movement of the glass substrate during the spray pyrolysis deposition process, which was caused by the pressure of the spray. It was also noted that the TiO_2 compact layer coated fully the FTO glass which was desirable in the fabrication of high efficient dye-sensitized solar cell.

Figure 2 shows the micrograph of TiO_2 nanoparticle film.

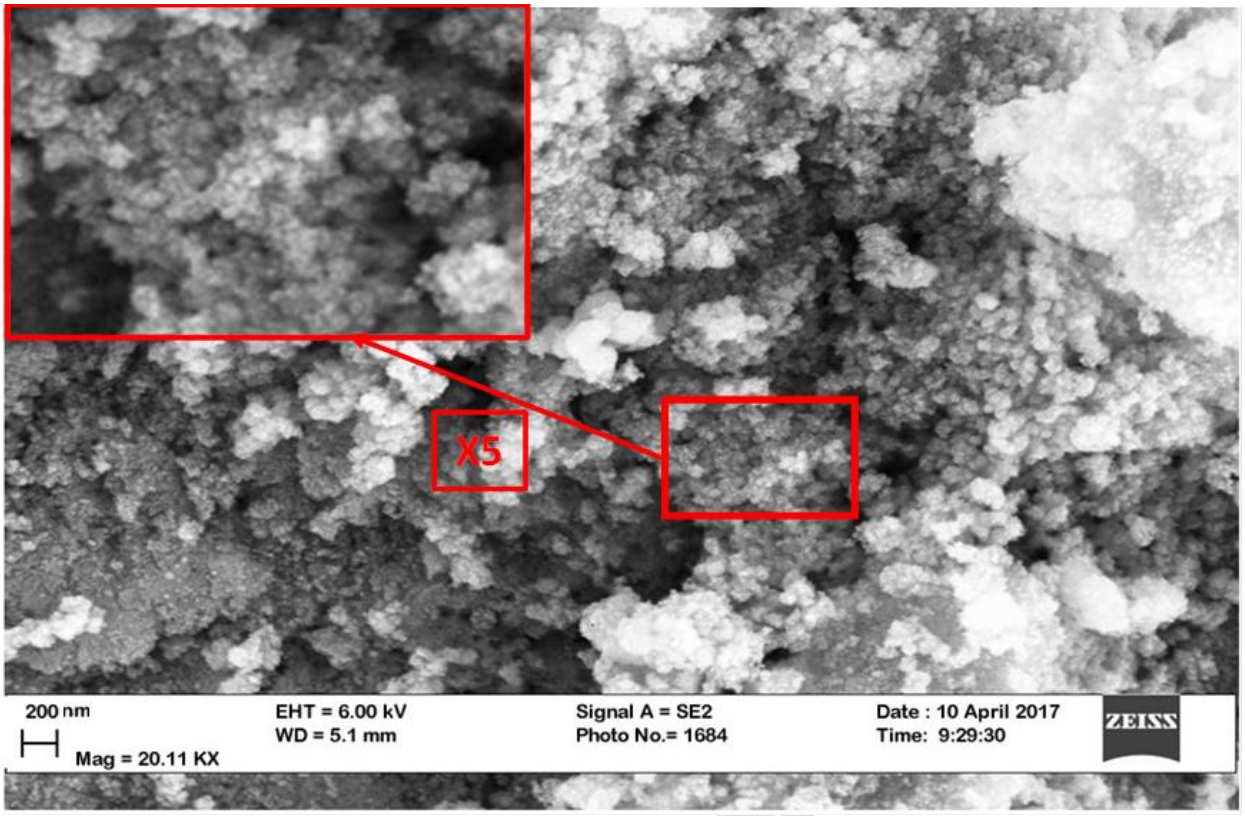

Figure 2 – SEM micrograph of TiO_2 nanoparticle film

From this figure, the nanoparticles were spongy and had unevenly sphere-shaped profile, which is an important factor to high performing DSSC fabricated out of these films. Due to the screen printing method of film deposition, was little film uniformity which is evident due to dark and bright areas. Figure 3 shows that TiO_2 nanotubes had a skein-like morphology with abundant number of nanotubes intertwined together such that their surface area is really large.

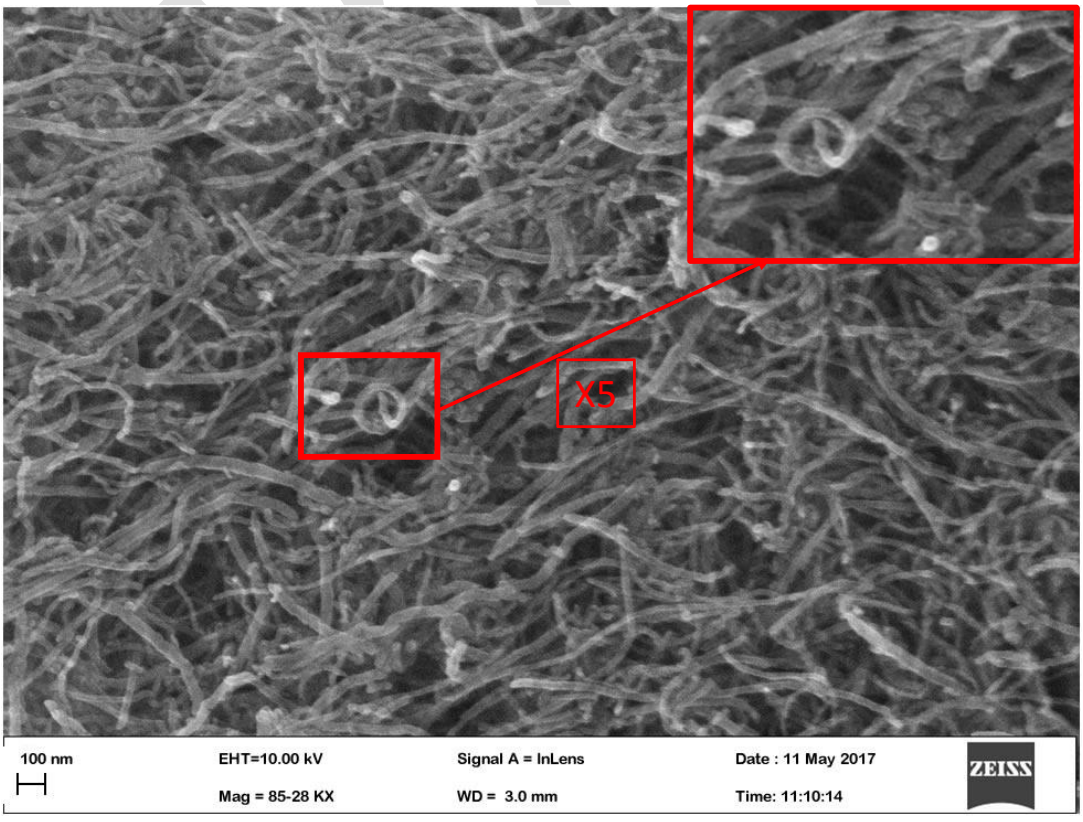

Figure 3 – SEM micrograph of TiO2 nanotubes

These skein-like nanotubes were produced due to the heat treatment of the precursor solutions at 110 °C for 20 hours.

Transmission and reflectance characteristics of TiO_2 thin films. Figure 4 represents transmission characteristics of the prepared TiO_2 films.

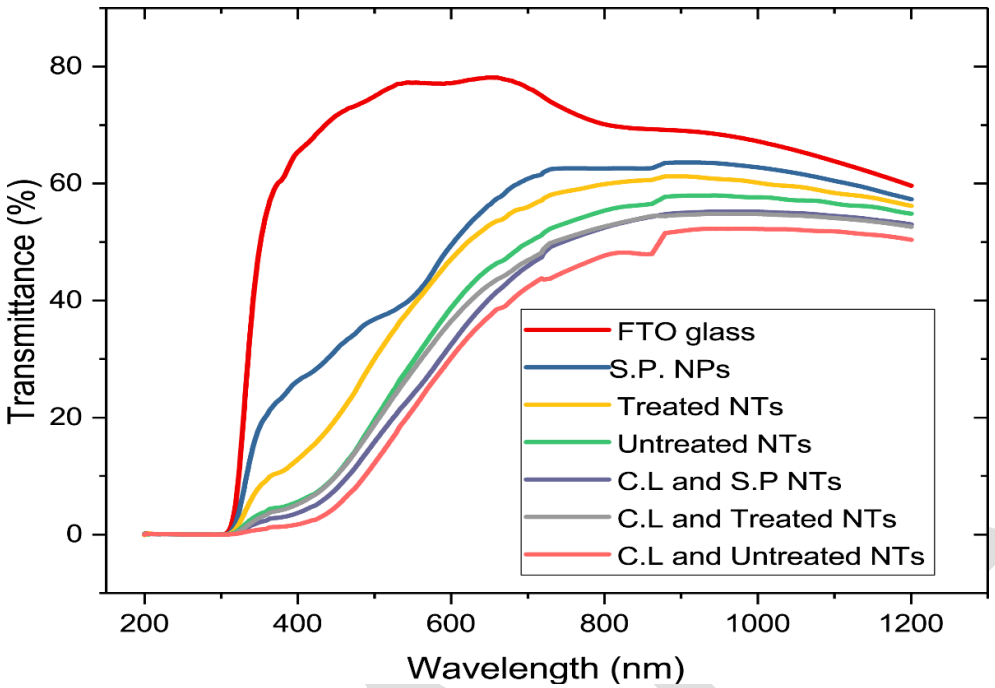

Figure 4 – Transmission characteristics of TiO_2 films prepared

This figure shows that treating titanium dioxide nanotubes with $TiCl_4$ slightly improves the transmission properties. This was attributed to the nanotube diameter since the treated nanotube has smaller diameter than that of untreated nanotube which allows more light to be transmitted in the treated nanotube than in the untreated nanotube. Nanotube diameter is determined by the water content in the TiO_2 nanotubes and treating them with $TiCl_4$ ensures that most of the water content is used up in the hydrolysis reaction that takes place. This minimizes the nanotube diameter consequently increasing the fraction of light transmitted [19].

In addition, introducing TiO_2 compact layer to both screen printed TiO_2 nanoparticle and TiO_2 nanotube films (whether treated or untreated) was found to reduce the transmittance as shown in Figure 4. Compact layer increased the film thickness which resulted to a larger fraction of light not being transmitted. As film thickness increases, the transmittance decreases because there are excess atoms which are introduced in the structure of the film. Increase in the number of atoms causes darkening of the interior part of the film and therefore lesser portion of light photons can pass through the thick film as compared to the thin film [20].

Figure 5 shows the reflectivity characteristics of the prepared TiO_2 thin films where it was observed that all the films have low reflectance (less than 15% in the visible region on average). Moreover, it was observed that there were several peaks in most of the curves which were attributed to the multiple reflection effect the three interfaces of the air/thin film/transparent substrate bi-layer [18]. Multiple reflection happens because the overall reflectance is described by taking into account the product of the reflection co-efficient multiplied by the complex conjugate of the reflection.

Figure 5 also shows that at low wavelengths (not exceeding 250 nm), there was notably high reflectance than at all other wavelength marks which was attributed to high absorption at these wavelengths. This therefore meant that these thin films exhibited high absorption behavior which makes the material a good absorber material for solar cell applications.

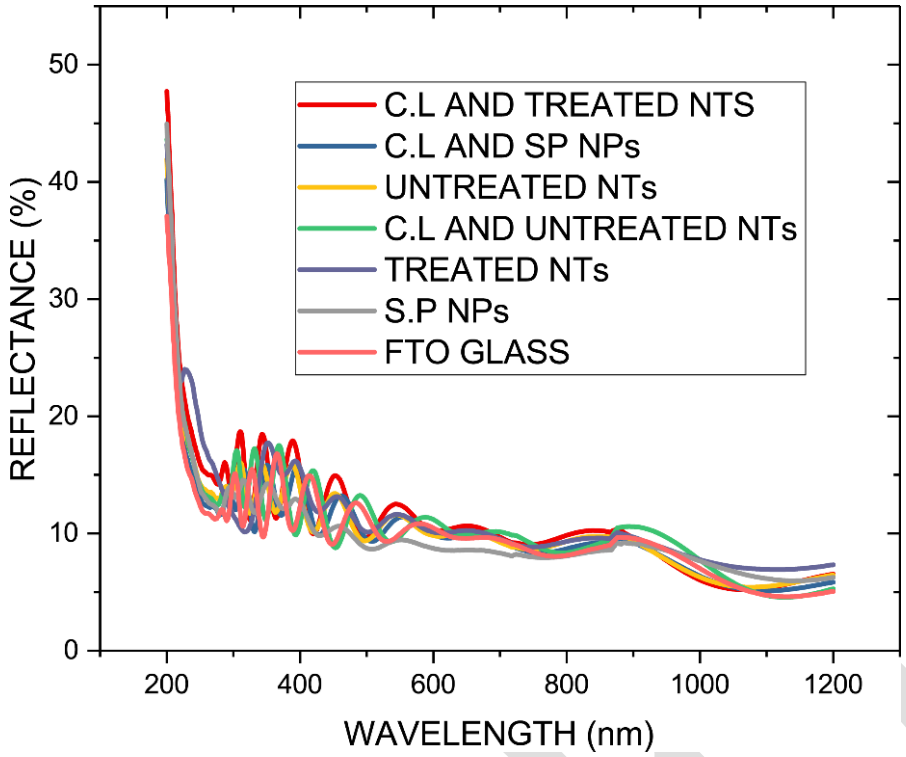

Figure 5 – Spectral plot of reflectance characteristics of TiO_2 thin films

Film thickness determination and comparison. The experimental data was fitted in to the simulated data to obtain the film thickness. At the point when the simulated curves were in good agreement with the experimental curves, it was possible to obtain the film thickness directly from the fit parameters section in the Scout software. In this study, the experimental value of the film thickness was also compared with the film thickness value obtained from the simulation using Scout software models.

Figure 6 shows the plots for the transmission characteristics and the simulated graphs against wavelength for all the titanium dioxide films fabricated.

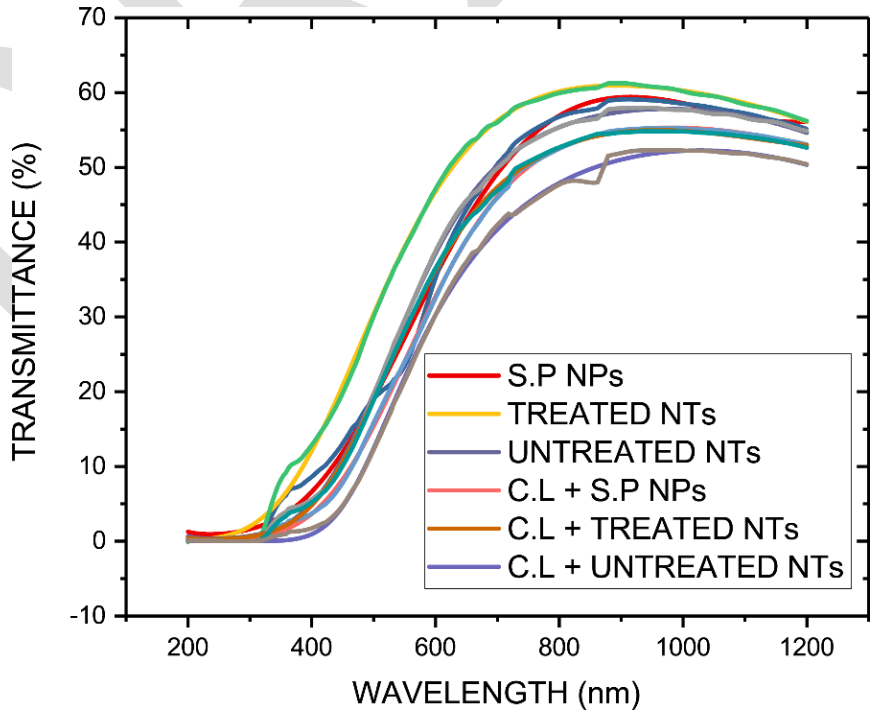

Figure 6 – Combined fitting of simulated versus experimental transmittance data

There was very good agreement between the simulated and experimental graphs and hence film thickness values tabulated in Table 1 were got. Table 1 includes the film thicknesses obtained by using Scout software which have been compared (with their percentage error) from the film thickness obtained from the KLA-Tencor *Alpha-Step* IQ Surface *Profilometer*.

Table 1 – Summary of prepared thin films and their film thicknesses

Sample N.	Description	Simulated film thickness (nm)	Measured film thickness (nm)	Percentage difference (%)
O	Screen printed nanoparticles	116	116.06	0.052
N	$TiCl_4$ treated TiO_2 nanotubes	122.9	122.88	0.016
K	Untreated TiO_2 nanotubes	150.0	150.0	0
J	TiO_2 compact layer + screen printed TiO_2 nanoparticles	152.4	152.38	0.013
H	TiO_2 compact layer + treated TiO_2 nanotubes	156.9	156.88	0.013
L	TiO_2 compact layer + untreated TiO_2 nanotubes	159.5	159.48	0.012

Absorption coefficient. Figure 7 shows the plots of absorption coefficient against the incident radiation energy. At low energies (high wavelengths) TiO_2 films had very low absorption coefficients and at high light energies, there was high absorption coefficients of these films.

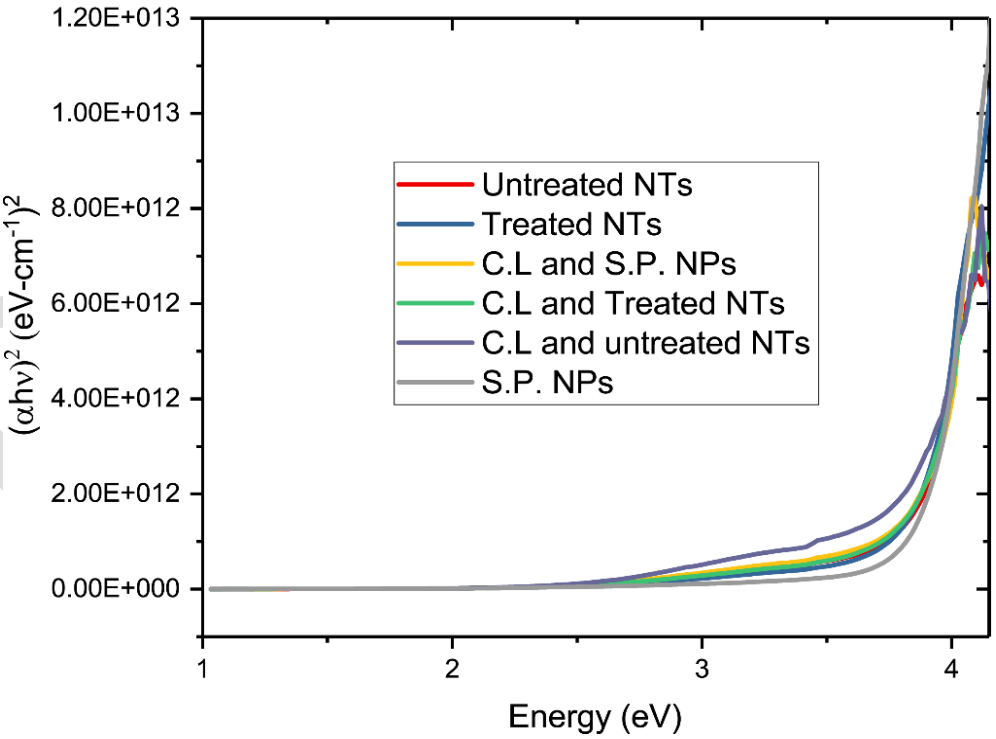

Figure 7 – Plots for absorption coefficient against energy

This meant that the films were translucent to light at wavelengths not exceeding 370 nm because the energy possessed by the light had not exceeded the band gap energy of TiO_2 and therefore electrons could not be excited from the valence band to the conduction band in the TiO_2 band structure. Moreover, this physical phenomenon was attributed to the light absorption at the grain boundaries [21].

Optical band gap. TiO_2 has been known to be a semiconductor with has got both indirect and direct band gaps [22]. The direct optical band gap for the TiO_2 films fabricated was obtained by plotting $(\alpha h\nu)^2$ against energy of the incident light and extrapolating $(\alpha h\nu)^2$ to zero. In determination of direct band gap, direct transitions were assumed and therefore Equation (6) was used [22].

$$(\alpha h\nu)^2 = A\left(h\nu - E_g\right) \quad (6)$$

Figure 8 shows that TiO_2 films had a direct band gap energy of 3.81 eV which agreed closely to literature [23].

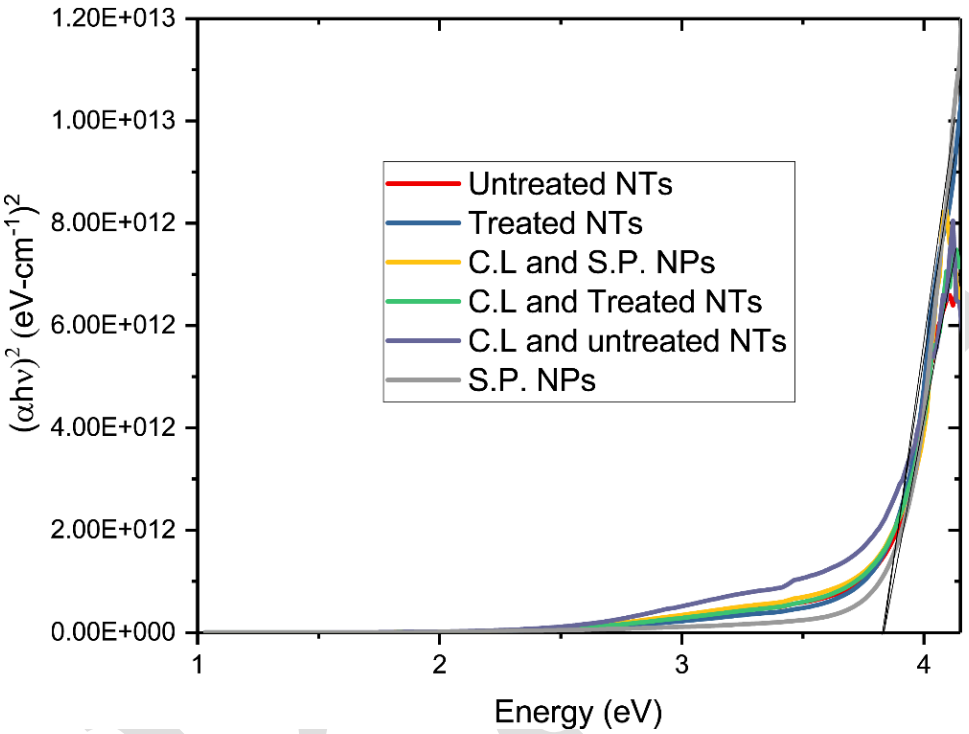

Figure 8 – Plot of $(ahv)^2$ against energy for the direct gap energy determination

However, the value reported for anatase TiO_2 band gap energy is 3.39 eV [24] meaning that the band gap energy value obtained had a red-shift of 0.42 eV. This was attributed to the quantum-size (Q-size) effect on the TiO_2. As the size of the TiO_2 particles became small, the valence band was lowered and the conduction band was raised thereby widening the band gap. The TiO2 band gap blue-shift was in the acceptable range to the reported range of 0.1 to 0.6 eV [25].

Figure 9 represents a plot of $(\alpha h\nu)^{1/2}$ against $h\nu$ for the determination of the indirect band gap which was found to be 3.64 eV. This band gap energy value was very close to the reported value in literature [24].

OJL's model parameters. The OJL Mass was taken as the square root of the third power of the valence and conduction band masses. This is a parameter that acts as a scaling factor in the determination of the shape of the density of states and therefore small values of the OJL mass are the best. The smaller the OJL mass of electrons, the higher the electron mobility [26].

Table 2 shows that the higher the values of the OJL mass, the higher the values of OJL Gap energy (E_0) which agreed well with literature [27]. The possible reason for this correlation was thought to be due to the decay function in the OJL model which minimized the spectral weight at higher energies in order to make the integral over the whole spectral range finite.

The difference between the energy at the conduction band and the energy at the valence band was taken to give the Gap energy (E_0). The Gap energy was got when the damping constants of the conduction band (gC) and valence band (gV) are zero [16].

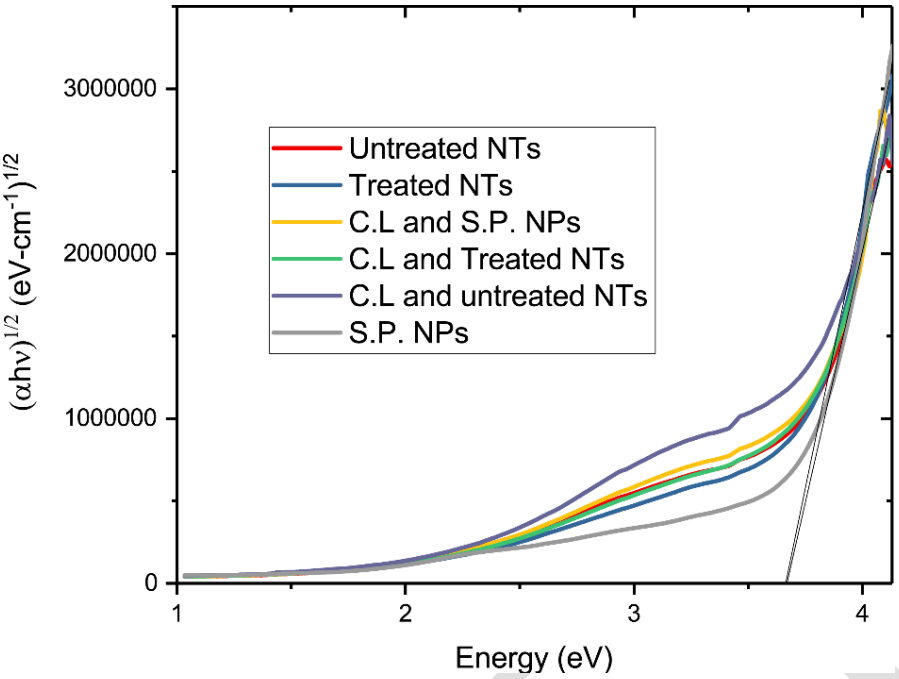

Figure 9 – Indirect band gap determination plots

The OJL Gap energy (E_0) values were obtained to be between 30273.2356 and 31072.0000 wavenumbers as seen in Table 2. These values translated to band-gap energies between 3.744 and 3.843 eV which were close to value reported in literature [27].

Table 2 – Summary of electronic inter-band transition parameters

Sample No	Description	OJL Mass	OJL decay	OJL Gap energy (E_0)	OJL Gamma valence band	OJL Ratio.
O	Screen printed nanoparticles	0.1773	52035.6992	30273.2356	678.2379	0.8676
N	$TiCl_4$ treated TiO_2 nanotubes	0.1792	49225.3008	30722.2563	684.0625	0.8941
K	Untreated TiO_2 nanotubes	0.3262	25132.7305	30898.9785	1089.0930	1.4610
J	TiO_2 compact layer + screen printed nanoparticles	0.2800	29976.5625	30868.7660	490.1338	0.8026
H	TiO_2 compact layer + treated TiO_2 nanotubes	0.3639	25751.1348	31072.0000	1585.2480	1.7450
L	TiO_2 compact layer + untreated TiO_2 nanotubes	1.0913	60933.5313	31225.7845	1587.8186	1.9922

The Gamma valence (represented by gV) shows the extent to which damping at the valence band occurs when one assumes the parabolic bands for the crystalline material. In this case, the tail exponentially decays into the band gap [16]. From table 2, it is important to note that gV values' range is restricted since too small values would lead to difficulties in the dielectric function calculation.

The OJL Ratio is the ratio of gV to gC. This parameter is a constant as it shows the extent of damping for both the valence and conduction band exponential decays. As shown in Table 2, the Gamma valence band (gV) values showed that damping at the valence band took place at a rate between 490.1338 and 1587.8186. In this case, the TiO_2 samples were taken to have parabolic bands in their structure. These values have a good range which is required in the dielectric function calculation.

The dielectric function usually has two parts; the imaginary and the real part. The density of states

(DOS) of the CB and VB is proportional to the dielectric function's imaginary part. In cases where modification lacks, dielectric function's imaginary part increases to infinity as the energy increases. For this reason, the dielectric function's real part construction by the Fourier transforms becomes difficult and this demands a decay factor to be included to drag down the imaginary part to zero for high frequencies. The OJL Decay is a number that governs the way the imaginary part decays to zero for high frequencies[14].

From Table 2, the OJL decay number for the six TiO_2 samples was found to be high enough (over 25000 1/cm) which indicated that the imaginary part of the dielectric function decayed to zero at high frequencies well. This is necessary for the construction of the real part of the dielectric function.

The ratios of the exponential decay of the valence band to conduction band are as shown under the OJL ratio column in Table 2. Ratios higher than 1 indicate that conduction band decay occurred at a faster rate than the valence band decay while ratios less than 1 show that the valence band decay was faster than the conduction band decay.

CONCLUSION

TiO_2 thin films were successfully synthesized using sol-gel and hydrothermal methods. The SEM micrographs confirmed that spongy nanoparticles and skein-like nanotubes were formed, which is a good attribute of a film to be used in DSSC fabrication. The optical characterization done on the TiO_2 thin films showed the effect of introducing compact layer and post-treatment of TiO_2 nanotubes with $TiCl_4$ to transmittance. In addition, this analysis showed that TiO_2 thin films had both direct and indirect band-gaps. The OJL Gap energy (E_0) values were obtained to be between 30273.2356 and 31072.0000 wavenumbers. Moreover, the Gamma valence band (gV) values showed that damping at the valence band took place at a rate between 490.1338 and 1587.8186.

ACKNOWLEDGEMENTS

The authors wish to acknowledge solid state laboratories, University of Nairobi, for the technical support during the optical measurements of the samples and Chemistry department, Kenyatta University for availing chemicals used in this work. In addition, African Development Bank is hereby acknowledged for providing the corresponding author with a scholarship which enabled these studies to be conducted.

REFERENCES

1. O'Regan, B., & Grätzel, M. (1991). A low-cost, high-efficiency solar cell based on dye-sensitized colloidal TiO2 films. *Nature, 353*(6346), 737–740. doi: 10.1038/353737a0
2. Martirosyan, A., & Schneider, Y.-J. (2014). Engineered Nanomaterials in Food: Implications for Food Safety and Consumer Health. *International Journal of Environmental Research and Public Health, 11*(6), 5720–5750. doi: 10.3390/ijerph110605720
3. Zhang, Y., Leu, Y.-R., Aitken, R., & Riediker, M. (2015). Inventory of Engineered Nanoparticle-Containing Consumer Products Available in the Singapore Retail Market and Likelihood of Release into the Aquatic Environment. *International Journal of Environmental Research and Public Health, 12*(8), 8717–8743. doi: 10.3390/ijerph120808717
4. Bedikyan, L., Zakhariev, S. & Zakharieva, M. (2013). Titanium Dioxide Thin Films: Preparation and Optical Properties. *Journal of Chemical Technology and Metallurgy, 48*(6), 555–558.
5. Mawyin, J. (2009). *Characterization of Anthocyanin Based Dye-Sensitized Organic Solar Cells (DSSC) and Modifications Based on Bio-Inspired Ion Mobility Improvements* (Doctoral thesis). Retrieved from http://adsabs.harvard.edu/abs/2009PhDT.....291M
6. Malekshahi Byranvand, M., Nemati Kharat, A., & Fatholahi, L. (2012). Influence of nanostructured TiO_2 film thickness on photo-electrode structure and performance of flexible Dye-Sensitized Solar Cells. *Journal of Nanostructures, 2*, 327–332.

7. Atif, M., Farooq, W., Fatehmulla, A., Aslam, M., & Ali, S. (2015). Photovoltaic and Impedance Spectroscopy Study of Screen-Printed TiO_2 Based CdS Quantum Dot Sensitized Solar Cells. *Materials, 8*(1), 355–367. doi: 10.3390/ma8010355

8. Viana, M. M., Mohallem, T. D. S., Nascimento, G. L. T., & Mohallem, N. D. S. (2006). Nanocrystalline titanium oxide thin films prepared by sol-gel process. *Brazilian Journal of Physics, 36*(3b), 1081–1083. doi: 10.1590/s0103-97332006000600075

9. Sima, C., Waldhauser, W., Lackner, J., Kahn, M., Nicolae, I., Viespe, C., Grigoriu, C., & Manea, A. (2007). Properties of TiO2 thin films deposited by RF magnetron sputtering. *Journal of Optoelectronics and Advanced Materials, 9*, 1446–1449.

10. Mathur, S., & Kuhn, P. (2006). CVD of titanium oxide coatings: Comparative evaluation of thermal and plasma assisted processes. *Surface and Coatings Technology, 201*(3-4), 807–814. doi: 10.1016/j.surfcoat.2005.12.039

11. Hanaor, D., Michelazzi, M., Veronesi, P., Leonelli, C., Romagnoli, M., & Sorrell, C. (2011). Anodic aqueous electrophoretic deposition of titanium dioxide using carboxylic acids as dispersing agents. *Journal of the European Ceramic Society, 31*(6), 1041–1047. doi: 10.1016/j.jeurceramsoc.2010.12.017

12. Li, H., Liu, H., Fu, A., Wu, G., Xu, M., Pang, G., … Zhao, X. (2016). Synthesis and Characterization of N-Doped Porous TiO2 Hollow Spheres and Their Photocatalytic and Optical Properties. *Materials, 9*(10), 849. doi: 10.3390/ma9100849

13. Mosiori, C. O., Maera, J., Shikambe, R., … Magare, R. (2017). Electrical Behavior of Cd0.3Zn1.1x S0.7 Thin Films for Non-Heat Light Emitting Diodes. *Path of Science, 3*(6), 2.8–2.16. doi: 10.22178/pos.23-5

14. Gopinadhan, K., Kashyap, S. C., Pandya, D. K., & Chaudhary, S. (2007). High temperature ferromagnetism in Mn-doped SnO2 nanocrystalline thin films. *Journal of Applied Physics, 102*(11), 113513. doi: 10.1063/1.2817825

15. Kasuga, T., Hiramatsu, M., Hoson, A., Sekino, T. and Niihara, K. (1999). Titania nanotubes prepared by chemical processing, Advanced Materials, 11, 1307-1311. Doi: abs/10.1002/(SICI)1521-4095(199910)11

16. W. Theiss. (n. d.). *Thin film analyis with SCOUT*. Retrieved June 1, 2018, from http://www.mtheiss.com/?c=2&content=applications_scout

17. Liu, X., Guo, M., Cao, J., Lin, J., Tsang, Y., Chen, X., & Huang, H. (2014). Large-diameter titanium dioxide nanotube arrays as a scattering layer for high-efficiency dye-sensitized solar cell. *Nanoscale Research Letters, 9*(1), 362. doi: 10.1186/1556-276x-9-362

18. Shariffudin, S. S., Salina, M., Herman, S. H., & Rusop, M. (2012). Effect of Film Thickness on Structural, Electrical, and Optical Properties of Sol-Gel Deposited Layer-by-layer ZnO Nanoparticles. *Transactions on Electrical and Electronic Materials, 13*(2), 102–105. doi: 10.4313/teem.2012.13.2.102

19. Outemzabet, R., Bouras, N., & Kesri, N. (2007). Microstructure and physical properties of nanofaceted antimony doped tin oxide thin films deposited by chemical vapor deposition on different substrates. *Thin Solid Films, 515*(16), 6518–6520. doi: 10.1016/j.tsf.2006.11.069

20. Solieman, A. S., Hafiz, M. M., Abu-Sehly, A. A., & Alfaqeer, A. A. (2014). Dependence of optical properties on the thickness of amorphous Ge30Se70 thin films. *Journal of Taibah University for Science, 8*(3), 282–288. doi: 10.1016/j.jtusci.2014.01.002

21. Ziabari, A. A., & Ghodsi, F. E. (2012). Surface morphology and optoelectronic studies of sol–gel derived nanostructured CdO thin films: heat treatment effect. *Journal of Materials Science: Materials in Electronics, 23*(9), 1628–1639. doi: 10.1007/s10854-012-0640-x

22. Ghrairi, N., & Bouaicha, M. (2012). Structural, morphological, and optical properties of TiO2 thin films synthesized by the electro phoretic deposition technique. *Nanoscale Research Letters, 7*(1), 357. doi: 10.1186/1556-276x-7-357

23. Ahmadi, K., Abdolahzadeh Ziabari, A., Mirabbaszadeh, K., & Ahmadi, S. (2015). Synthesis of TiO_2 nanotube array thin films and determination of the optical constants using transmittance data. *Superlattices and Microstructures, 77*, 25–34. doi: 10.1016/j.spmi.2014.10.024

24. Janitabar-Darzi, S., Mahjoub, A. R., & Nilchi, A. (2009). Investigation of structural, optical and photocatalytic properties of mesoporous TiO_2 thin film synthesized by sol–gel templating technique. *Physica E: Low-Dimensional Systems and Nanostructures, 42*(2), 176–181. doi: 10.1016/j.physe.2009.10.006

25. Satoh, N., Nakashima, T., Kamikura, K., & Yamamoto, K. (2008). Quantum size effect in TiO2 nanoparticles prepared by finely controlled metal assembly on dendrimer templates. *Nature Nanotechnology, 3*(2), 106–111. doi: 10.1038/nnano.2008.2

26. Huang, F. (2010). Titanium Dioxide Nanomaterials: Basics and Design, Synthesis and Applications in Solar Energy Utilization Techniques. *Solar Collectors and Panels, Theory and Applications*. doi: 10.5772/10339

27. Gordijn, A., Löffler, J., Arnoldbik, W. M., Tichelaar, F. D., Rath, J. K., & Schropp, R. E. I. (2005). Thickness determination of thin (~20 nm) microcrystalline silicon layers. *Solar Energy Materials and Solar Cells, 87*(1-4), 445–455. doi: 10.1016/j.solmat.2004.09.016